ACS APPLIED MATERIALS & INTERFACES

www.acsami.org

Research Article

Bioengineered Lab-Grown Meat-like Constructs through 3D Bioprinting of Antioxidative Protein Hydrolysates

Sayan Deb Dutta, Keya Ganguly, Min-Soo Jeong, Dinesh K. Patel, Tejal V. Patil, Seong-Jun Cho, and Ki-Taek Lim*

Cite This: *ACS Appl. Mater. Interfaces* 2022, 14, 34513−34526

Read Online

ACCESS | Metrics & More | Article Recommendations | Supporting Information

ABSTRACT: Lab-grown bovine meat analogues are emerging alternatives to animal sacrifices for cultured meat production. The most challenging aspect of the production process is the rapid proliferation of cells and establishment of the desired 3D structure for mass production. In this study, we developed a direct ink writing-based 3D-bioprinted meat culture platform composed of 6% (w/v) alginate and 4% (w/v) gelatin (Alg/Gel)-based hydrogel scaffolds supplemented with naturally derived protein hydrolysates (PHs; 10%) from highly nutritive plants (soybean, pigeon pea, and wheat), and some selected edible insects (beetles, crickets, and mealworms) on in vitro proliferation of bovine myosatellite cells (bMSCs) extracted from fresh meat samples. The developed bioink exhibited excellent shear-thinning behavior ($n < 1$) and mechanical stability during 3D bioprinting. Commercial proteases (Alcalase, Neutrase, and Flavourzyme) were used for protein hydrolysis. The resulting hydrolysates exhibited lower-molecular-weight bands (12−50 kDa) than those of crude isolates (55−160 kDa), as determined by sodium dodecyl sulfate-polyacrylamide gel electrophoresis. The degree of hydrolysis was higher in the presence of Alcalase for both plant (34%) and insect (62%) PHs than other enzymes. The 3D-printed hydrogel scaffolds displayed excellent bioactivity and stability after 7 days of incubation. The developed prototype structure (pepperoni meat, 20 × 20 × 5 mm) provided a highly stable, nutritious, and mechanically strong structure that supported the rapid proliferation of myoblasts in a low-serum environment during the entire culture period. The 2,2-diphenyl-1-picrylhydrazyl radical scavenging assay enhanced the free radical reduction of Alcalase- and Neutrase-treated PHs. Furthermore, the bioprinted bMSCs displayed early myogenesis (desmin and Pax7) in the presence of PHs, suggesting its role in bMSC differentiation. In conclusion, we developed a 3D bioprinted and bioactive meat culture platform using Alg/Gel/PHs as a printable and edible component for the mass production of cultured meat.

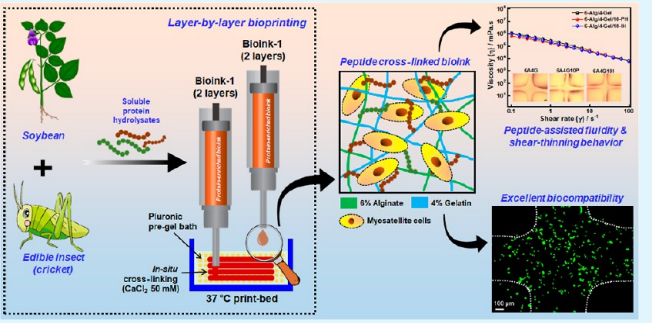

KEYWORDS: *lab-grown meat, protein hydrolysate, 3D bioprinting, antioxidant, bioactive platform*

1. INTRODUCTION

Bovine meat (beef) production is one of the most demanding businesses in the 21st century owing to the global population increase, which is expected to reach 9−10 billion by 2050. Global meat consumption has increased over time in certain regions of the world, including Asia and Latin America. In contrast, some countries, such as Europe and North America, have exhibited relatively stable or slightly decreasing meat consumption patterns over the past few years.[1] To fulfill the increased demand of meat, traditional livestock-based meat production will require additional resources, such as water, crops, and land; however, these resources are already largely consumed by humans.[2−5] Therefore, an effective alternative strategy is required to address the limitations of livestock-based meat production and meet the increasing demand of meat worldwide. Cultured meat can resolve this problem by minimizing livestock-related farming issues. According to the Intergovernmental Panel on Climate Change in Switzerland, cultured meat is an effective alternative to reduce global climate change and provide a sustainable environment. The key advantages of cultured meat production involve three factors: sustainability, animal welfare, and human health.[6,7]

With the advent of tissue engineering, cell-based meat (CBM) (also known as cultured, cultivated, lab-grown, or clean meat) production has increased with the aim of producing meat from cell cultures and minimizing unnecessary animal sacrifices.[8,9] Recently, CBM has drawn considerable attention from an ethical standpoint to environmental safety and public health; however, it is still under debate.[10] Although

Received: June 15, 2022
Accepted: July 6, 2022
Published: July 18, 2022

most CBMs are based on plant-based scaffolding systems,[9] the nutrition facts (e.g., protein percentage, amount of calories, and process quality) have yet to be taken into consideration when compared with real meat. In most cases, CBMs are mixed with flavoring agents (e.g., benzaldehyde, ethyl butyrate, and acetoin),[11] adipocytes (fat cells), and myoblasts (muscle cells), and then textured.[10] CBMs combined with the above-mentioned components can raise serum cholesterol (approximately 20%), elevate blood pressure (20−30%),[12] and may lead to the development of several diseases, such as pulmonary hypertension (9−37%),[12] hyperlipidemia, and colorectal cancers,[13] which are related to high protein/fat diets and characterized by an increased body mass index.[14,15] To date, there are two main strategies for CBM production: direct manipulation of bovine muscle cells, which includes the isolation, expansion, and mass production of bovine muscle cells, or generation of muscle progenitors from induced pluripotent stem cells cultured using a bioreactor.[16] The first method is considered safe for human consumption.[17−19] The nutritional value of cultured meat also depends greatly on the cryoprotectants used for storage. The cytoprotective effects of functional foods have long been studied because of their vital role in scavenging cellular oxidative stress. Oxidative stress is caused by the accumulation of reactive oxygen species, such as superoxide anions (O^-), hydroxyl anions (OH^-), and hydrogen peroxide (H_2O_2) inside the cells, which play a significant role in the development of diseases such as obesity, cancer, and cardiovascular diseases.[20,21] Therefore, the use of antioxidative proteins that ameliorate oxidative stress and have a high nutritional value is one of the primary goals for the successful commercialization of cultured meat. The synthetic antioxidants used for meat production (butylated hydroxyanisole and butylated hydroxytoluene) have potential risks, including liver damage and many others.[22] Thus, the development of naturally derived antioxidants is crucial for greater health benefits.

Naturally derived nonprotein components, such as polyphenols and alkaloids, are often used as sources of antioxidants.[22] Naturally derived protein hydrolysates (PHs) have gained considerable attention owing to their high nutritional and antioxidative properties. PHs contain several bioactive peptides that act as stress-reducing agents. PHs can be obtained from various protein sources such as mushrooms,[23] fish fins and scales,[24,25] porcine skin,[26] soybeans,[27] milk,[27,28] pigeon peas,[29] potatoes,[28] and edible insects.[30] In addition, PHs (peptide fragments or cryptides) are widely recognized as antioxidative molecules present inside cells.[31] Therefore, a combination of plant or insect protein meal can be used as a nutritive source of myoblast proliferation and differentiation. Table 1 shows the nutritive value of conventional bovine meat and its alternatives in terms of sustainability. Recently, an innovative approach for clean meat was introduced by Tsuruwaka and Shimada using fish fin cells and was described as a potential alternative for conventional meat.[25] Previously, plant-derived proteins in combination with biopolymer scaffolds were shown to improve the proliferation and differentiation potential of muscle stem cells for cultured meat production. Ianovici et al.[32] reported a 3D printing technique using pea and soy protein isolates (PPI and SPI) with alginate/RGD protein that increased muscle cell proliferation by up to 90%. In another study, wheat glutenin was used as a nutritive source of rat myoblast cells for cultured meat production.[5] However, raw proteins extracted from natural sources often exhibit poor water solubility, hindering their extensive use for scaffold fabrication.[1,32] In addition, many recently published reports have explored the use of murine-derived myoblast cell culture techniques, which are practically inconvenient and do not resemble beef.

Table 1. Nutritive Value of Conventional Cow Meat and Its Alternatives in Terms of Sustainability[16]

description	% of uncooked protein/100 g	energy/100 g (uncooked)
conventional beef	14−22 g	121−332 kcal
faux beef meat	22 g	259 kcal
soy protein	81 g	0.338 kcal
mealworm	14−25 g	206 kcal

This study focuses on the 3D printing of an alginate-gelatin-based polymeric interface incorporating PHs of plants (*Glycine max*, soybean; *Cajanus cajan*, pigeon pea; and *Triticum vulgare*, wheat gluten extract) and insects (*Protaetia brevitarsis*, beetle; *Gryllus bimaculatus*, cricket; and *Tenebrio molitor*, mealworm) for the production of lab-grown meat analogues. A mixture of plant proteins with alginate as a bioink was previously demonstrated in some studies.[32−34] However, the use of thermoresponsive alginate-gelatin bioink composed of plant or insect proteins has not been previously assessed for 3D bioprinting of bovine muscle cells. Alginate is a brown algae-derived polysaccharide used extensively in tissue engineering owing to its tunable mechanical properties and high cytocompatibility.[35] Gelatin, a hydrolysis product of collagen, is also a widely used scaffolding material owing to its unique degradability, cytocompatibility, and low systemic toxicity.[36] In this study, we developed a 3D printable shear-thinning hydrogel bioink composed of alginate and gelatin (Alg−Gel) as a scaffolding material and PHs as a nutritive supplement (antioxidative and proliferative agent) for innovative cost reduction of cultured meat. We used different commercial proteases (Alcalase, Neutrase, and Flavourzyme) to hydrolyze *G. max*, *C. cajan*, *T. vulgare*, *P. brevitarsis*, *G. bimaculatus*, and *T. molitor* protein isolates. Figure 1 shows a schematic illustration of 3-printed CBM production using the polysaccharide-protein-based hybrid platform. Finally, as a *proof-of-concept*, we bioprinted bovine myosatellite cells (bMSCs) using PHs-enriched bioink and demonstrated the in vitro biocompatibility and myoblast differentiation, which directly resembles cultured beef meat. We anticipate that the developed 3D structure will be an excellent prototype for the production of lab-grown meat at a commercial level with added antioxidants from naturally derived functional PHs; the present study is a step toward clean meat development.

2. MATERIALS AND METHODS

2.1. Materials. Plant-derived protein isolates (soybean, pea, and gluten) were obtained from Pingdingshan Tianjin Plant Albumen Co. Ltd. (Pingdingshan, China), the Green Labs LLC (Clifton, New Jersey, USA), and ADM Chamtor Ltd. (Bazancourt, France). The protease enzymes, including Alcalase (2.4 L), Neutrase (0.8 L), and Flavourzyme (1000 L), were procured from Novozymes Ltd., Bagsvaerd, Denmark. Insect samples (*P. brevitarsis*, *G. bimaculatus*, and *T. molitor*) were obtained from a local farm (Godae farm, Wonju, Republic of Korea).

2.2. Preparation and Characterization of PHs. *2.2.1. Preparation of Plant Protein Hydrolysates.* Plant-derived PHs were prepared as reported elsewhere.[37] Briefly, the 3 commercial protein isolates were hydrated with 20-fold of sterile distilled water and pasteurized at

https://doi.org/10.1021/acsami.2c10620
ACS Appl. Mater. Interfaces 2022, 14, 34513−34526

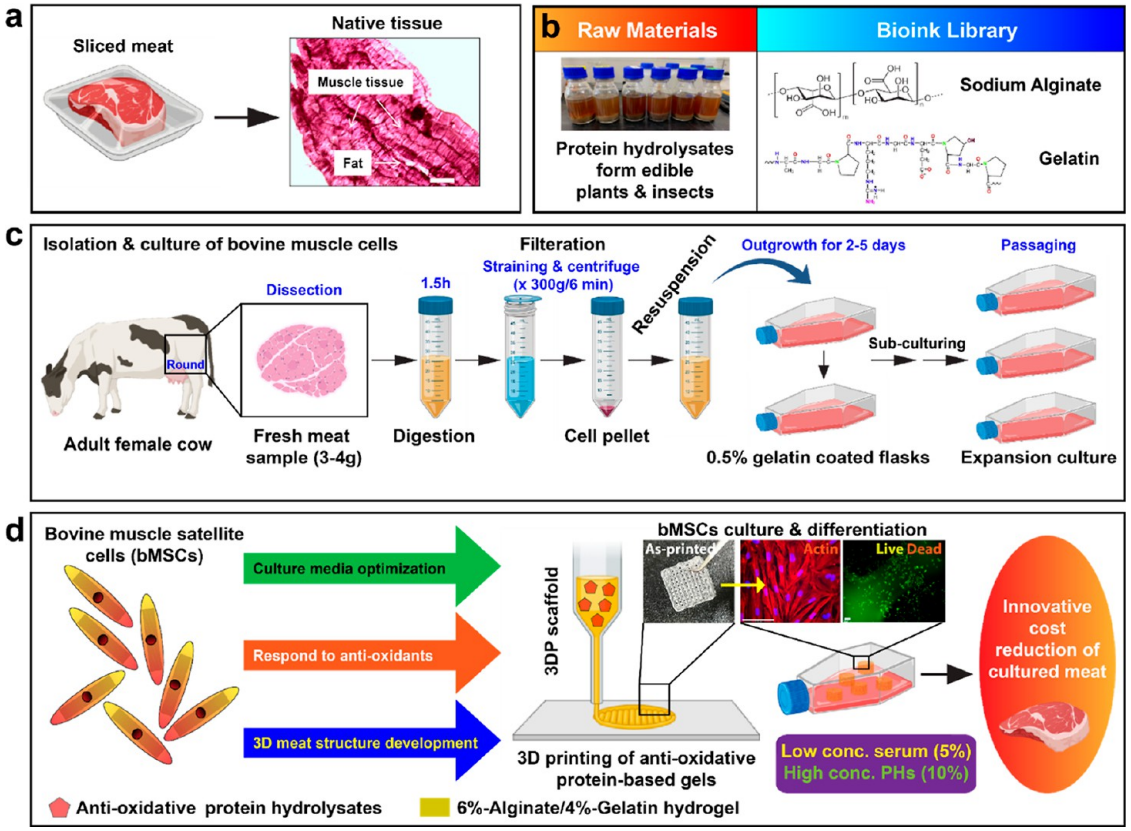

Figure 1. Overview of the cow-free meat production strategy. (a) Structure of the sliced meat. The H&E staining of the native meat tissue showing the presence of muscle and fat cells. Scale bar: 100 μm. (b) Extracted bioactive PHs from edible plants and insects used in this study. The bioink library which consist of 3D printable biopolymers (sodium alginate and gelatin) used in this study. (c) Schematic representation for the isolation, culture, and maintenance of the bovine muscle satellite cells (bMSCs) from slaughtered cow meat. (d) Schematic illustration for the cell preparation, culture media optimization, 3D printing, and development of cow-free meat constructs for innovative cost reduction of cultured meat.

90 °C for 15 min under vigorous stirring. Next, the temperature was brought to 50 °C, and the enzyme solution was slowly added to the pasteurized solution. The resulting mixture was allowed to react for 12 h at 50 °C. After enzymatic digestion, the reaction was stopped by heating the mixture at 100 °C for 20 min. Next, the mixture was allowed to cool down at room temperature and purified by centrifuging at 3,220*g* for 15 min, followed by filtration.

2.2.2. Preparation of Insect Protein Hydrolysates. The insect protein isolates were prepared, as reported in our previous study.[30] The preparation process for insect protein hydrolysates (IPHs) is similar to plant protein hydrolysates (PPHs), as mentioned above. The list of plant- and insect-derived protein isolates and their names are listed in Table S1.

2.2.3. Estimation of Molecular Weight. The molecular weight of the PPHs and IPHs was determined by the sodium dodecyl sulfate-polyacrylamide gel electrophoresis (SDS-PAGE) method. Briefly, the electrophoresis was conducted using a 5% stacking gel with 60 V current and 10% separating gel with 100 V current, respectively. Next, the gels were stained with 0.05% Coomassie brilliant blue (Sigma-Aldrich, USA) and destained using a destining solution (acetic acid:methanol:deionized water; 2:5:5, v/v/v). The images were captured using ChemiDox XRS+ (Bio-Rad Laboratories, Hercules, CA, USA), and the band intensity was quantified using Image Lab software (v6.0, Bio-Rad, USA).

2.2.4. 2,2-Diphenyl-1-picrylhydrazyl Radical Scavenging Activity. The hydrolysates' antioxidant property was determined using the 2,2-diphenyl-1-picrylhydrazyl (DPPH) assay reported elsewhere with some modifications.[21] Briefly, 10% of PHs were prepared in a DPPH solution (0.4 mM), vortex for 10 s, and incubated for 30 min in the dark at room temperature. A spectrophotometer measured the absorbance at 517 nm every 10 min interval over 60 min. 1% ascorbate (Sigma-Aldrich, USA) solution was prepared as the control and compared with the test samples.

2.4. In Vitro Biocompatibility of PHs. *2.4.1. Cell viability Assay.* The cell viability of the bMSCs was evaluated by the WST-8 assay. For this, passage 1 or 3 bMSCs (1×10^4 cells/100 μL media) were cultured on 96-well plates in the presence of growth media. After that, the cells were supplemented with 100 μL of 10% PPHs and IPHs + 5% FBS containing media and cultured for 24 and 48 h. After the desired incubation, the cells were washed by PBS and supplemented with fresh media. Culture plates containing only 5% FBS were considered as the control. Finally, the cells were incubated with 100 μL of WST-8 dye (Cellrix Viability Assay Kit, Republic of Korea) and incubated for 2 h. The reacted formazan was quantified using a microplate reader at 450 nm (625 nm as a reference value). All experiments were performed in triplicate (n = 3), and data are presented as mean ± s.d.

2.4.2. Effect of PHs on Myogenic Differentiation. The effects of PPHs and IPHs on myobalstic-protein marker expression were evaluated using the immunocytochemical (ICC) technique. For this, the cells (2.5×10^4 cells/500 μL media) were cultured in confocal dishes and treated with 10% PPHs and IPHs for 3 days. The media with only 5% FBS was taken as the control. The staining procedure was described in our previous studies.[30,35] Briefly, the cells were fixed with 3.7% paraformaldehyde (PFA) for 15 min at room temperature, followed by permeabilization with Triton-X 100 (0.1%) for 10 min. After that, the cells were blocked by 1% BSA for 1 h and incubated with specific primary and secondary antibodies against desmin and myogenin. The nucleus was counterstained by DAPI solution for 1−2 min in the dark and visualized with an inverted fluorescence microscope (DMi8, Leica Microsystems, Wetzlar, Germany). The images were captured at high-resolution mode and processed with Image-Pro 6.0 software (Leica Microsystems, Wetzlar, Germany).

https://doi.org/10.1021/acsami.2c10620
ACS Appl. Mater. Interfaces 2022, 14, 34513−34526

2.5. Preparation of Composite Bioink. Alginate−gelatin (Alg−Gel) hydrogel was prepared as reported previously.[35] Briefly, sodium alginate powder (Sigma-Aldrich, USA) was dissolved in distilled water at a concentration of 6% (w/v) at 70 °C, followed by an addition of 4% (w/v) fish gelatin (Sigma-Aldrich, USA) at 45 °C. A fixed concentration of each PH [10%; (v/v)] was added to the hydrogels. The hydrogel devoid of the PH served as the control group. The as-prepared hydrogels were filled into a printing cartridge and stored at 4 °C overnight to initiate gelation. The bioink composition and their corresponding names are given in Table S2.

2.6. Bioink Characterization. The chemical interaction of the PHs was studied using a Fourier transform infrared (FT-IR) spectrophotometer (Perkin Elmer, UK). The viscoelastic nature of the developed bioink was evaluated using a rotational rheometer (MCT92, Anton Paar, Austria) with 10 mm parallel plates at 25 °C. The frequency sweep test (ω) was performed within 0.1 to 100 R s^{-1} with 1% strain rate. The shear-thinning test was performed within 0.1 to 100 s^{-1} shear range ($\dot{\gamma}$) with 10 Rad s^{-1} frequency rate, respectively. The mechanical property of the 3D-printed scaffolds were performed using a tensile machine (UTM, A&D Digital, Japan) under uniaxial compressive loading. The surface morphology of the printed scaffolds was examined by field-emission scanning electron microscopy (FE-SEM) (S400, Hitachi, Japan). An inverted optical microscope was used to monitor the printability of the hydrogels. The image analysis was performed using ImageJ software (v1.8, NIH, Bethesda, USA).

2.7. 3D Printing and Printability Evaluation. The 3D printing was performed using a commercial 3D printer (CELLINK BIO-X, Sweden) with motorized *Z*-axis. All the printed structures were designed using SOLIDWORKS software (Dassault Biosystems, France) and sliced using an open-source software (Slic3r). The circular (1 × 1 × 0.5 cm) and square (2 × 2 × 0.5 cm)-shaped structures with varying infill densities (20, 30, 40, and 80%) were printed using a 27-G metal head nozzle (inner dimeter 200 μm) with 5 mm/s speed. The 3D printing was performed in a cooled print-bed (10 ± 2 °C) with an average extrusion pressure of 120 ± 2 kPa. After 3D printing, the printed constructs were dipped into a 100 mM $CaCl_2$ bath for 5−10 min to initiate the ionic cross-linking. Next, the cross-linked hydrogel was rinsed with sterile PBS or distilled water to remove the excess Ca^{2+} and stored at 4 °C until further use. The printability was measured in terms of expansion factor (α = filament diameter/nozzle diameter) and pore uniformity factor (P_u = pore dimeter of the printed structure/pore diameter of the theoretical design), as described in our previous study.[35] The printing accuracy was calculated using following eq 1

$$\text{Printing accuracy (\%)} = \left(1 - \frac{(A_i - A)}{A}\right) \times 100 \quad (1)$$

where, A_i is the printed pore area and A is the theoretical area of the CAD structure as measured by ImageJ software.

2.8. 3D Bioprinting and Myogenic Induction of bMSCs. For 3D bioprinting, the bioinks (6-Alg/4-Gel, 6-Alg/4-Gel/10-PH, and 6-Alg/4-Gel/10-IH) were prepared in sterile Dulbecco's modified Eagle's medium (DMEM) and UV sterilized for 30 min. After that, the bioinks were mixed carefully with 0.2 mL of bMSCs to obtain a final concentration of 2.5 × 10^4 cells/mL cell density. Next, the bMSC-laden bioinks were loaded into the printing cartridges and kept at 37 °C to ensure minimal cell death. The supporting bath pre-gel was prepared using 30% Pluronic in DMEM media supplemented with 50 mM $CaCl_2$. Prior to 3D printing, the Pluronic pre-gel solution cast in a mold and incubated at 37 °C to initiate gelation. After complete gelation, the supporting bath gel was transferred onto the printing bed and the temperature was maintained around 37 ± 2 °C. After that, the pre-incubated bioink was carefully printed (1 × 1 × 0.5 cm structure) within the Pluronic bath gel. The printing was conducted layer-by-layer using two different cartridges where the first two layers were printed by bioink-1 (bMSCs + hydrogel) and the another two layer was printed using bioink-2 (bMSCs + hydrogel). The extruded liquid bioink immediately turned into cross-linked hydrogel owing to the presence of Ca^{2+} ions. Next, the printed constructs were carefully removed from the Pluronic bath and rinsed with cold PBS to remove the debris of Pluronic and additionally cross-linked with 100 mM $CaCl_2$ for 1−2 min. After cross-linking, the printed constructs were supplemented with fresh DMEM media and incubated at 37 °C with a 5% CO_2 chamber.

The viability of the bMSCs-laden hydrogels was assessed using the live/dead assay after 24 h of culture as reported in our previous study.[38] For myogenic induction, the bioprinted constructs were supplemented with DMEM/Glutamax-I media and cultured for 14 days. The media was replaced every after 3 days. After 14 days, the myogenic populations were identified via immunogenic marker staining. For this, the bioprinted constructs were carefully washed with PBS and fixed with 3.7% PFA for 15 min. After fixation, the constructs were permeabilized using 0.1% Triton-X 100, followed by blocking with 1% BSA for 1 h. After blocking, the bioprinted constructs were incubated with primary antibodies against desmin (1:200) and Pax7 (1:200), followed by incubation with Alexa Fluor-conjugated secondary antibodies. The cytoskeleton was stained with F-actin probe and nucleus was stained with DAPI. To observe the early accumulation of Pax7 in the nucleus, a colocalization experiment was performed to ensure the expression of Pax7. The images were captured using an inverted fluorescence microscope (DMi8, Leica, Germany) and the images were analyzed using Image-Pro 6 software (Leica, Germany).

2.9. Statistical Analysis. Statistical analysis was performed using the OriginPro 9.0 software (Origin Lab, USA). Statistical significant between the control and experimental groups was determined using one-way ANOVA and student's t-test. All the data are presented as mean ± s.d. of triplicated experiments (n = 3), statistical significant at $^*p < 0.05$ and $^{**}p < 0.01$.

3. RESULTS AND DISCUSSION

3.1. Characterization of Protein Hydrolysates. The hydrolase treatment usually generates short peptide fragments and is one of the most effective methods of hydrolysate preparation. In this regard, the degree of hydrolysis (DH) is one of the widely used indicators for comparing proteolysis. As shown in Figure S1a,b, we obtained higher DH for soybean (∼34%) and worm (∼62%) isolates following Alcalase treatment than other enzymes. This was due to the better activity of the Alcalase enzyme that generated small PHs with superior functional and bioactive properties. Digital photographs of the hydrolysates are presented in Figure S1c. The molecular weights of the peptide fragments were analyzed using sodium dodecyl sulfate-polyacrylamide gel electrophoresis to confirm the hydrolysis process. The quantification values of band intensity for PPHs and IPHs are shown in Figures S2 and S3. The undigested samples of PPHs showed a characteristic band ranging from 12 to 160 kDa. Interestingly, the major bands disappeared after hydrolysis with Alcalase and Neutrase. The Flavourzyme-treated samples also exhibited a similar pattern. The different cleavage patterns of the protein isolates were closely related to the enzymes used and indicated hydrolysis effectiveness.[39,40] The enhancement of TCA-soluble peptide content and the absence of major bands in the presence of Alcalase, Neutrase, and Flavourzyme suggest that the PPIs and IPIs were sufficiently hydrolyzed.

Free radicals are metabolic byproducts that actively participate in the development of several diseases such as cancer and cardiovascular disease. Therefore, an antioxidative diet may protect the human body against oxidative stress-induced damage.[29] This study evaluated the antioxidant activities of PPHs and IPHs using the DPPH radical scavenging assay, and the results are presented in Figure S4. An ascorbic acid (1%) solution was used as a control. The

https://doi.org/10.1021/acsami.2c10620
ACS Appl. Mater. Interfaces 2022, 14, 34513−34526

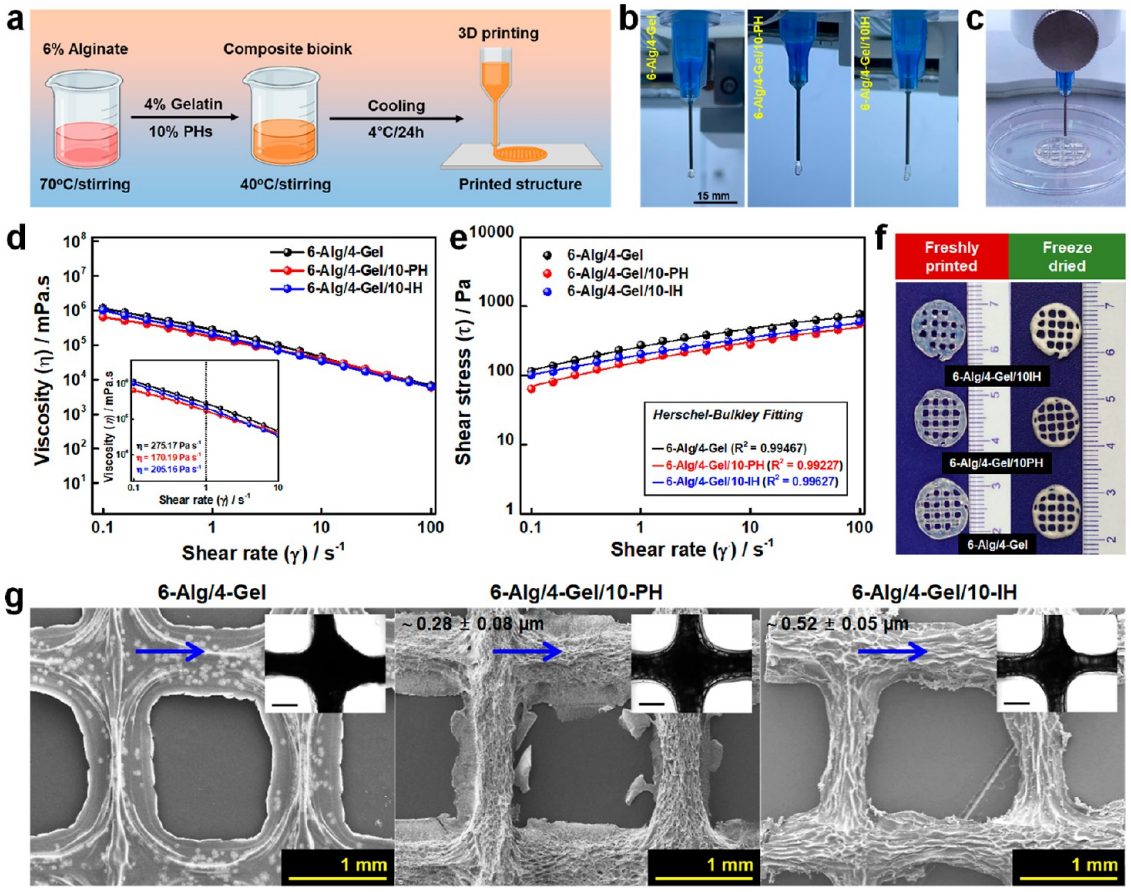

Figure 2. Formulation of bioink for 3D printing. (a) Schematic illustration for the bioink preparation composing the sodium alginate (Alg), gelatin (Gel), and PHs as a natural growth enhancer for bMSCs. (b) Representative photographs of filament formation test for different composite bioinks before 3D printing. (c) Digital photograph of the 3D printing process. The 3D printing was carried out using a temperature control printer-head and print-bed pre-incubated at 4 °C. (d,e) Shear-thinning property of the developed bioink. (f) Representative photographs of the 3D-printed meat constructs before (top) and after freeze-drying (bottom). (g) Scanning electron microscopy morphology of the freeze-dried 3D scaffolds with corresponding optical micrographs (inset) showing the porous nature of the scaffolds. The arrow head indicates the printing direction. Scale bar: 1 mm and 100 μm. Data are mean ± s.d. of triplicate experiments, statistical significance at $^*p < 0.05$ (Student *t*-test).

antioxidant properties of the 10% PPHs and IPHs changed over time, and an increasing tendency was observed in the Alcalase-treated plant hydrolysates (SPI and PPI), as shown in Figure S4a. Notably, the Flavourzyme-treated samples (GI) exhibited enhanced antioxidant activity compared with that of the SPI or PPI samples, indicating the radical scavenging potential of gluten isolates (Figure S4b). However, the IPHs showed alternate activity. The absorbance at 517 nm was dramatically changed in the Neutrase-treated samples compared with the Alcalase-treated samples, indicating that Neutrase hydrolysis generated more antioxidative peptides than Alcalase hydrolysis (Figure S4c−e). The antioxidant activity was likely due to the presence of specific amino acids (tryptophan, cysteine, methionine, and histidine) or peptides (cryptides) present in the PPHs and IPHs.[29,41,42] Similar observations from the literature suggest that low-molecular-weight peptides significantly induce antioxidant potential compared to larger peptides.[20,43] Digital photographs of DPPH reduction in the PPHs and IPHs are shown in Figure S5.

3.2. Physicochemical and Mechanical Characterization of Bioinks. A schematic illustration of the bioink fabrication and printing processes is shown in Figure 2a. The fabricated bioinks (6-Alg/4-Gel, 6-Alg/4-Gel/10-PH, and 6-Alg/4-Gel/10-IH) exhibited filament formation at ambient temperature (Figure 2b). A digital photograph of the 3D-printing process is shown in Figure 2c. The chemical interactions of the freeze-dried hydrogel scaffold were evaluated using FT-IR spectroscopy, and the results are shown in Figure S6. The FT-IR spectra of the Alg−Gel exhibited characteristic stretching vibrations at approximately 1590−1600 cm^{-1} owing to the presence of carboxylic (−C═O) and amine (−N−H) moieties in the amide-I region. Similarly, the appearance of absorption peaks around 1540 cm^{-1} (amide-II) corresponds to the strong interaction of the carboxylic moieties of alginate with the amine moieties of gelatin via amide bonding, as reported in our previous study.[35] Moreover, the addition of PHs and IHs exhibited no change in the absorbance at the amide-I and -II regions. Interestingly, a broad peak around 3265 cm^{-1} (−OH/−NH_2) in Alg/Gel was slightly shifted to the higher region (amide-X), indicating the interaction of PHs and IHs with Alg/Gel, as reported earlier.[44,45] Because the hydrolysates were small peptide fragments, the low-temperature gelation of Alg/Gel induced physical cross-linking of hydrolysates inside the polymer matrix. The printed scaffolds were cross-linked with 100 mM $CaCl_2$ for 30 min at RT. Digital images of the printed scaffolds are shown in Figure 2d. The viscoelastic properties of the

https://doi.org/10.1021/acsami.2c10620
ACS Appl. Mater. Interfaces 2022, 14, 34513−34526

fabricated bioinks were evaluated using a rotational rheometer with varying angular frequencies (ω) with 0.1 to 100 Rad s^{-1} range. A frequency sweep test was performed in the linear viscoelastic region to investigate the fluid nature of the bioink in the presence of PHs. Irrespective of the nanofiller type, a higher value of the storage modulus (G') corresponds to the elastic nature rather than the viscous nature of a given hydrogel ink.[46] Therefore, an ideal viscoelastic ink should have both sol−gel transition features under various conditions. We observed a decrease in the storage modulus (G') of the bioinks containing PHs 6-Alg/4-Gel/10-PH and 6-Alg/4-Gel/10-IH compared to that of bioinks with pure 6-Alg/4-Gel (Figure S7a). The gradual decrease in the storage modulus (G') of the hydrogels with PHs may have occurred because of the intercalation of the peptides (reduced packing of peptides in the polymer matrix) in the pure polymer matrix, thereby decreasing the interactive forces.[47] The G' values for 6-Alg/4-Gel, 6-Alg/4-Gel/10-PH, and 6-Alg/4-Gel/10-IH bioinks at 100 Rad s^{-1} were 8558.48, 2549.74, and 6057.10 Pa, respectively. The complex viscosity (η^*) of the fabricated hydrogel was measured between 0.1 and 100 Rad s^{-1}. As shown in Figure S7b, when the frequency was increased from 0.1 to 100 Rad s^{-1}, we observed a drastic change in the viscosity of the fabricated bioinks. The higher viscosity in the low-frequency region and lower viscosity in the high-frequency region demonstrate the shear-thinning and -thickening properties of the hydrogel inks.[35] Notably, the change in viscosity of 6-Alg/4-Gel/10-PH was greater than that of other bioinks owing to the greater intercalation of the peptide fragments, which increased the flowability of the bioink in the high-frequency region.

An ideal 3D printable bioink must have a shear-thinning property during extrusion from the nozzle and must quickly deposit onto the platform to form the desired structure.[48,49] Alg−Gel bioink has been shown to exhibit a concentration-dependent shear-thinning behavior during extrusion-based 3D printing.[50] A typical shear-thinning hydrogel displays "plug-like flow" and "non-Newtonian flow" behavior under varying shear stress. The shear-thinning and stress-yielding properties of the developed bioinks were evaluated using the Ostwald−de Waele model (power-law equation) and the Herschel−Bulkley flow model, as follows

$$\eta = k\dot{\gamma}^{(n-1)} \tag{2}$$

$$\tau = \tau_0 + k\gamma^n \tag{3}$$

where η is the viscosity of the hydrogel bioink, k is the flow consistency index (the viscosity of the bioink at a shear rate of 1 s^{-1}), $\dot{\gamma}$ is the shear rate, n is the shear-thinning index, and $\tau_0$is the yield stress. As shown in Figure 2d, the developed hydrogels exhibited excellent shear-thinning behavior with an increase in the shear rate ($\dot{\gamma}$) from 0.1 to 100 s^{-1}. All hydrogel bioinks exhibited excellent shear-thinning properties at $n < 1$. The shear-thinning indices for 6-Alg/4-Gel, 6-Alg/4-Gel/10-PH, and 6-Alg/4-Gel/10-IH were 0.43, 0.52, and 0.47, respectively, which is consistent with previous reports.[50] Moreover, our developed hydrogel displayed superior stress-yielding properties within the measured shear range. In this regard, the yield stress (τ_0), flow index (k), and shear-thinning index (n) showed the best fit to the Herschel−Bulkley flow model (Figure 2e), with a higher Pearson's R^2 value ($R^2 >$ 0.98), which was similar to the previously reported meat analogues.[51] Taken together, our results demonstrate that the developed hydrogel bioinks based on PHs have all the desired features for 3D printing with stress-yielding properties. Digital photographs of the 3D printed hydrogels are shown in Figure 2f. The mechanical properties of the 3D-printed scaffolds were evaluated via uniaxial compressive loading, and the results are shown in Figure S8. Notably, the PH-enriched scaffolds exhibited higher compressive strength than pure 6-Alg/4-Gel scaffolds (Figure S8a) even after swelling for 6 h (Figure S8b). The Young's modulus and ultimate tensile strength (Figure S8c,d) was obtained higher in the case of 6-Alg/4-Gel/10-PH (σ = 0.068 ± 0.03 MPa and E = 0.32 ± 0.05 MPa) and 6-Alg/4-Gel/10-IH (σ = 0.18 ± 0.05 MPa and E = 0.36 ± 0.05 MPa) scaffolds than pure 6-Alg/4-Gel (σ = 0.021 ± 0.008 MPa and E = 0.29 ± 0.02 MPa), which resembles the mechanical strength of the skeletal muscle.[52] We also observed a decrease in the tensile strength of all the scaffolds after equilibrium swelling owing to the greater hydrophilicity and water content of the scaffolds after the addition of PHs.

The morphology of the freeze-dried scaffolds was evaluated using FE-SEM, and the results are shown in Figure 2g. Interestingly, the PH-containing scaffolds (6-Alg/4-Gel/10-PH and 6-Alg/4-Gel/10-IH) exhibited an porous and flaky morphology compared with the pure 6-Alg/4-Gel scaffolds, indicating that the incorporation of PH-induced porosity. We observed a slight increase in porosity for 6-Alg/4-Gel/10-PH (~0.28 ± 0.08 μm) and 6-Alg/4-Gel/10-IH (~0.52 ± 0.05 μm) than pure 6-Alg/4-Gel. Moreover, upon hydrolysate addition, the surface of the scaffolds generated a homogenous primary structure with short or intermingled porous structures with desirable mechanical strength, which is crucial for skeletal cell growth.[53] The small and evenly distributed porous material therefore helps in greater adhesion and differentiation of skeletal muscle cells within the scaffold. In this regard, we anticipate that the formation of a uniformly distributed porous topology in PH-enriched scaffolds would promote enhanced nutrient uptake (PHs) and oxygen availability to skeletal cells and allow them to grow properly.[54] The swelling property of the prepared hydrogels was observed for a period of 48 h until equilibrium swelling was reached. An increase in swelling behavior was observed in the presence of PH-containing scaffolds compared with the pure 6-Alg/4-Gel scaffold (Figure S9). This was due to the soluble and hydrophilic components of the hydrolysates contributing to the overall swelling of the scaffolds.[44]

3.3. Printability of the Developed Bioink. The excellent shear-thinning and stress-yielding properties of the developed hydrogels motivated us to scrutinize their printing properties and shape fidelity. The shear-thinning property of the hydrogels incorporated with PHs was reflected in the printed constructs, showing a reduced expansion ratio in the experimental sets with respect to the 6-Alg/4-Gel hydrogel (Figure S10a). Optical micrographs of the printed hydrogels at the cross-connection (junction) and individual strands (bridge) are shown in Figure S10b. Notably, all the printed structures exhibited uniform filament formation without any collapse. This was also reflected in the porosity of the printed structures. We obtained negligible differences in the pore uniformity (Figure S10c) of pure 6-Alg/4-Gel and its composite bioinks after 3D printing and $CaCl_2$ cross-linking, demonstrating that all formulated bioinks had excellent print stability, which is crucial for tissue engineering.[35,55]

The outstanding printability, surface topography, and swelling properties of the developed bioinks motivated us to

https://doi.org/10.1021/acsami.2c10620
ACS Appl. Mater. Interfaces 2022, 14, 34513−34526

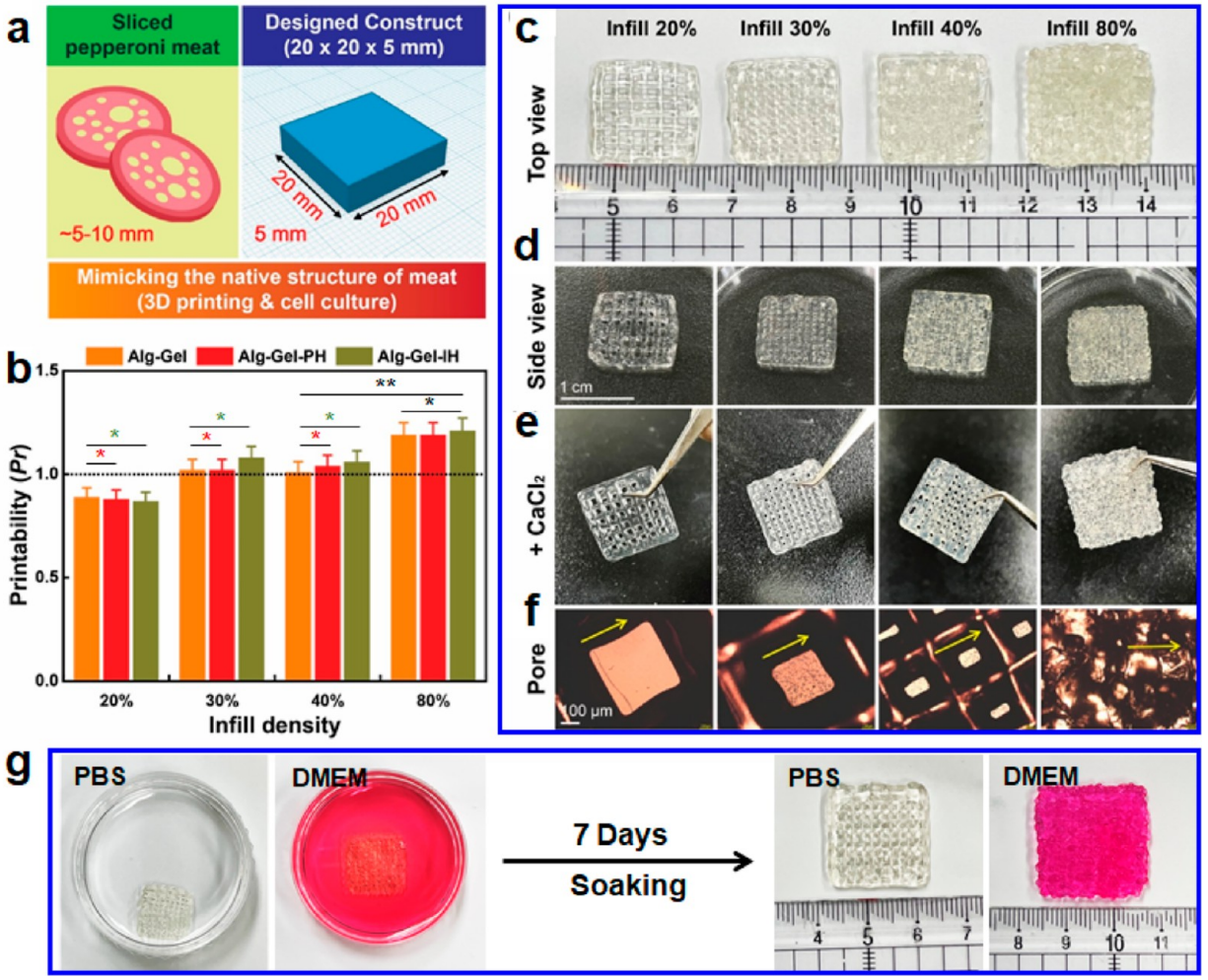

Figure 3. Biomimicking the sliced meat for 3D printing and printability optimization. (a) Pictorial representation of the sliced pepperoni meat (5−10 mm thick) and the mimicking CAD model (20 × 20 × 5 mm). (b) Optimization of printability factor (*Pr*) for designing the bioengineered pepperoni meat construct. (c) Representative 3D printed constructs with varying infill densities (20, 30, 40, and 80%) showing the stability of printing. (d,e) 3D-printed constructs showing the porous nature after $CaCl_2$ (100 mM) cross-linking. Scale bar: 1 cm. (f) Representative optical microscopy images of the printed constructs showing the printing direction and pore uniformity. Scale bar: 100 μm. (g) Shape changes of the printed constructs soaked in PBS and DMEM media for 7 days at 37 °C. Data are mean ± s.d. of triplicate experiments, statistical significance at $^*p < 0.05$ and $^{**}p < 0.01$ (Student *t*-test).

fabricate 3D meat prototypes. Kang et al. previously demonstrated 3D printing of tendon gel-integrated bioprinting with a total of 72 fibers comprising 42 muscle, 28 adipose, and 2 blood capillary samples to mimic the native meat tissue.[10] As discussed previously, our study focused on the fabrication of fat-free meat analogues; therefore, we excluded the whole meat concept and only focused on the concept of sliced thin meat. We were motivated to print-sliced "pepperoni meat" used extensively in restaurants for pizza or burger making. Commercial pepperoni meat has a thickness of 5−10 mm depending on the cut (Figure 3a). Therefore, as a proof-of-concept, we designed an identical structure with a dimension of 20 mm (length) × 20 mm (width) × 5 mm (thickness). We designed various infill densities (20−80%) to evaluate the printing performance. Notably, the printability (*Pr*) of all the hydrogels increased with an increase in the infill density of the constructs (Figure 3b). *Pr* close to 1 was observed at an infill density of 30% for the Alg−Gel and Alg−Gel-PH hydrogels. The Alg−Gel-IH hydrogel had a higher *Pr* value under similar conditions. Digital photographs of the printed pepperoni constructs with increased infill densities are shown in Figure 3c,d. We observed nearly accurate printing efficiency with varying infill density. The printing accuracy was calculated ~84.85% for 20% infill pattern, while it was ~80.54% for 80% infill and no pore was found in the case of 100% infill density constructs (Figure S11). In this regard, the scaffolds retained their pore dimensions even after cross-linking with $CaCl_2$ (Figure 3e,f). The reduced printing accuracy is due to the short travelling distance of the nozzle and coalesce of adjacent strands as reported in the previous literature.[56] Therefore, we used a recti-linear geometry with 20% infill density for 3D bioprinting experiments to minimize the strand fusion. Furthermore, we examined the stability of the printed hydrogels after 7 days of soaking in PBS and DMEM; they showed no obvious degradation at 37 °C, indicating the good structural stability (Figure 3g).

3.4. Characterization and Media Optimization of bMSCs. We observed increased viability of the bMSCs as the passage increased from P_0 to P_3 (Figure 4a). This was due to the inherent capability of cells to express a variety of transcription factors that regulate cell growth. We isolated bMSCs from adult female cows and cultured them for 2 weeks.

https://doi.org/10.1021/acsami.2c10620
ACS Appl. Mater. Interfaces 2022, 14, 34513−34526

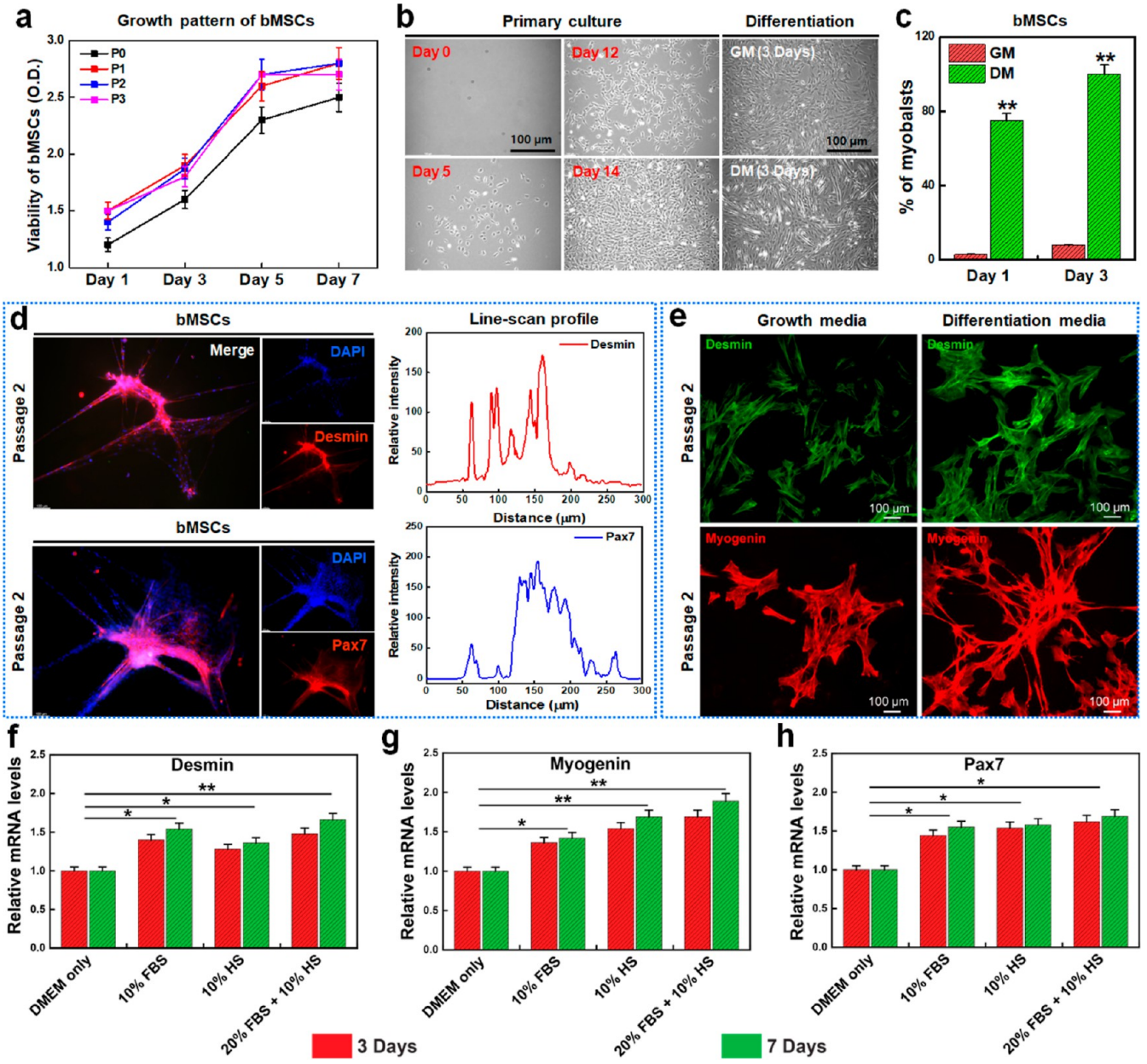

Figure 4. Characterization and media optimization of bMSCs. (a) Growth curve (proliferation rate) of bMSCs at different passages (P_0 to P_3) was evaluated using the WST-1 assay viability test (n = 3) after 7 days of incubation. (b) Representative optical photographs of the bMSC primary culture (DMEM medium + 10% FBS), expansion culture (DMEM Glutamax-I medium + 10% FBS), and differentiation study (DMEM Glutamax-I + 20% FBS + 10% HS) at indicated time points. (c) Calculation of myobalstic cells in growth (GM) and differentiation media (DM), n = 3. (d,e) Representative fluorescence images of bMSCs showing the expression of desmin and Pax7 after 3 days of culture in DM. Scale bar: 100 μm. (f–h) The relative mRNA expression of desmin, myogenin, and Pax7 following incubation in DMEM, 10% FBS, 10% HS, and 20% FBS + 10% HS, respectively (n = 3). Data are mean ± s.d. of triplicate experiments, statistical significance at $^*p < 0.05$ and $^{**}p < 0.01$ (Student t-test).

As shown in Figure 4b, the cells are initially round and grew properly in gelatin-coated T75 flasks within 7 days of primary culture. The outgrowth cells were comparatively smaller in size and exhibited fibroblast-like growth when cultured in growth media. Notably, the cells exhibited a typical myoblastic morphology when cultured in differentiation media (high-glucose DMEM + 20% FBS + 10% HS + 1% P/S). High glucose and serum supplementation facilitated myoblast differentiation, which is consistent with previous reports.[57]

bMSCs express various myogenic genes and protein markers, such as desmin, myogenin (MyoA and MyoD), and paxillin-7 (Pax7).[57−59] The cells were cultured to P_3 in growth and differentiation media to evaluate their protein marker expression. As shown in Figure 4c, the percentage of myoblastic cells increased significantly in the differentiation medium compared with that in the growth medium. The bMSCs (P_2) were stained with myoblast-specific markers to determine the presence of desmin- and Pax7-positive cells in both growth and differentiation media for 3 days. As shown in Figure 4d, the bMSCs were positive for both desmin and Pax7 markers when cultured in the growth medium. The relative fluorescence intensity was measured using a line-scan profile, suggesting an enhancement of the fluorescence intensities for desmin and Pax7. However, the desmin-positive cells appeared

https://doi.org/10.1021/acsami.2c10620
ACS Appl. Mater. Interfaces 2022, 14, 34513−34526

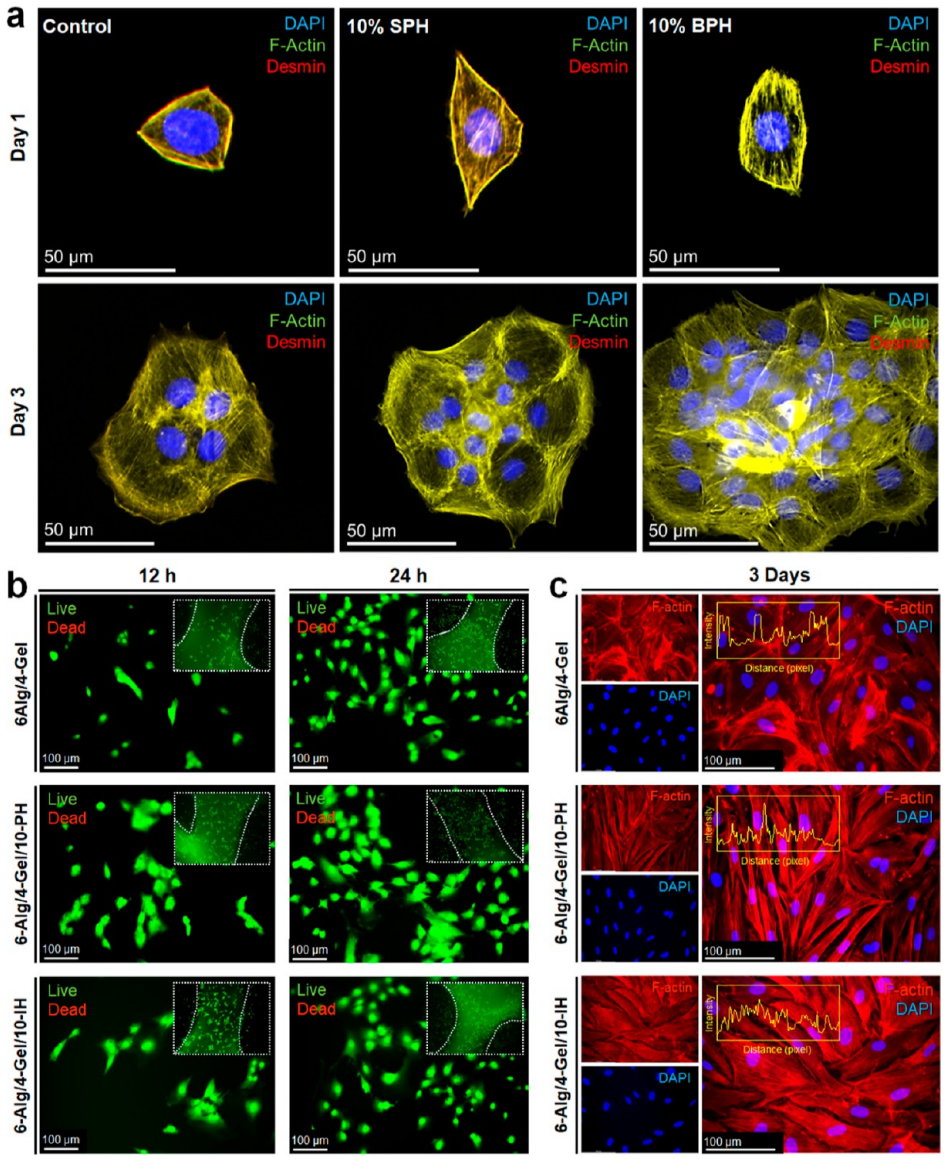

Figure 5. (a) Morphology of the bMSCs (DAPI/nucleus, F-actin/green, and desmin/red) in the presence of 10% SPH and 10% BPH after 3 days of incubation. 10% FBS containing media was taken as the control. (b) Representative live-dead (L/D) viability assay of bMSCs in the presence of Alg−Gel, Alg−Gel-PH, and Alg−Gel-IH at the indicated time intervals. (c) Fluorescence microscopy (FL) images of bMSCs showing the F-actin (red) arrangement with the corresponding FL intensities (insets) in the presence of 6-Alg/4-Gel, 6-Alg/4-Gel/10-PH, and 6-Alg/4-Gel/10-IH 3D scaffolds after 3 days of incubation. Scale bar: 50 and 100 μm.

aggregated and reduced myotube formation efficiency in the growth medium. Conversely, the expression of desmin and myogenin was significantly higher when cultured in the differentiation medium for 3 days. The increased cellular fluorescence in both desmin- and myogenin-positive cells exhibited long, filament-like morphology, suggesting the formation of early myotubes or myogenesis (Figure 4e).

To evaluate the growth of bMSCs in various media, we cultured the cells in a DMEM-Glutamax-I medium containing 10% FBS, 10% HS, and 20% FBS + 10% HS. Cells treated with DMEM alone were used as the control group. Next, the cells were cultured for the desired time period, and the expression of myogenic gene markers (*desmin*, *myogenin*, and *Pax7*) was evaluated using the real-time polymerase chain reaction. Notably, the expression of both *desmin* and *myogenin* was enhanced in the presence of 10% FBS, 10% HS, and 20% FBS + 10% HS. However, the 20% FBS + 10% HS group exhibited higher expression of *desmin* and *myogenin* than the other experimental groups, indicating that a combination of FBS and HS promotes the myogenic activity of bMSCs (Figure 4f,g). This was also reflected in the *Pax7* expression, where a significant increase in expression was observed in media containing 20% FBS + 10% HS (Figure 4h).

3.5. In Vitro Bioactivity of PHs and Myogenic Differentiation of bMSCs. The influence of PHs on the cytotoxicity of bMSCs was evaluated using the WST-8 assay after 48 h of culture, and the results are shown in Figure S12. The cells were cultured in 10% PPH- and IPH-supplemented media with 5% FBS. Plates containing 5% FBS were used as controls. Notably, the PPHs were found to be biocompatible, except for PPI(NH), of which the viability was slightly decreased. The viability of bMSCs was significantly increased ($p < 0.05$) in the presence of SPI(NH) supplements compared with that in the control and other groups (Figure S12a). A

https://doi.org/10.1021/acsami.2c10620
ACS Appl. Mater. Interfaces 2022, 14, 34513−34526

Table 2. Comparative Study of 3D Scaffolds with Naturally Derived Extracts for Cultured Meat Production Described in the Literature

scaffold	nutritive source	fabrication technique	type of cells	references
textured soy protein scaffold	soy protein	hydrogel casting	bovine muscle satellite cells (bMSCs)	9
chitosan-cellulose	C-phycocyanine	nanofilm	mouse myoblast (C2C12)	7
gellan gum		supporting bath-assisted 3D bioprinting	bovine muscle (bMSCs) and adipocytes (bADs)	10
porous and fibrous glutenin sponge	wheat gluten	hydrogel casting	mouse myoblast (C2C12) and bovine satellite cells (bMSCs)	5
RGD-modified alginate	PPI and SPI	extrusion-based 3D printing	bovine mesenchymal stem cells (bMSCs)	32
fish fin-derived decellularized scaffold		multilayered cell molding	fish fin-derived muscle and fibroblast cells	25
6% alginate-4% gelatin	plant (soy bean) and edible insect (beetle) PHs	DIW-based 3D bioprinting	bovine muscle satellite cells (bMSCs)	present work

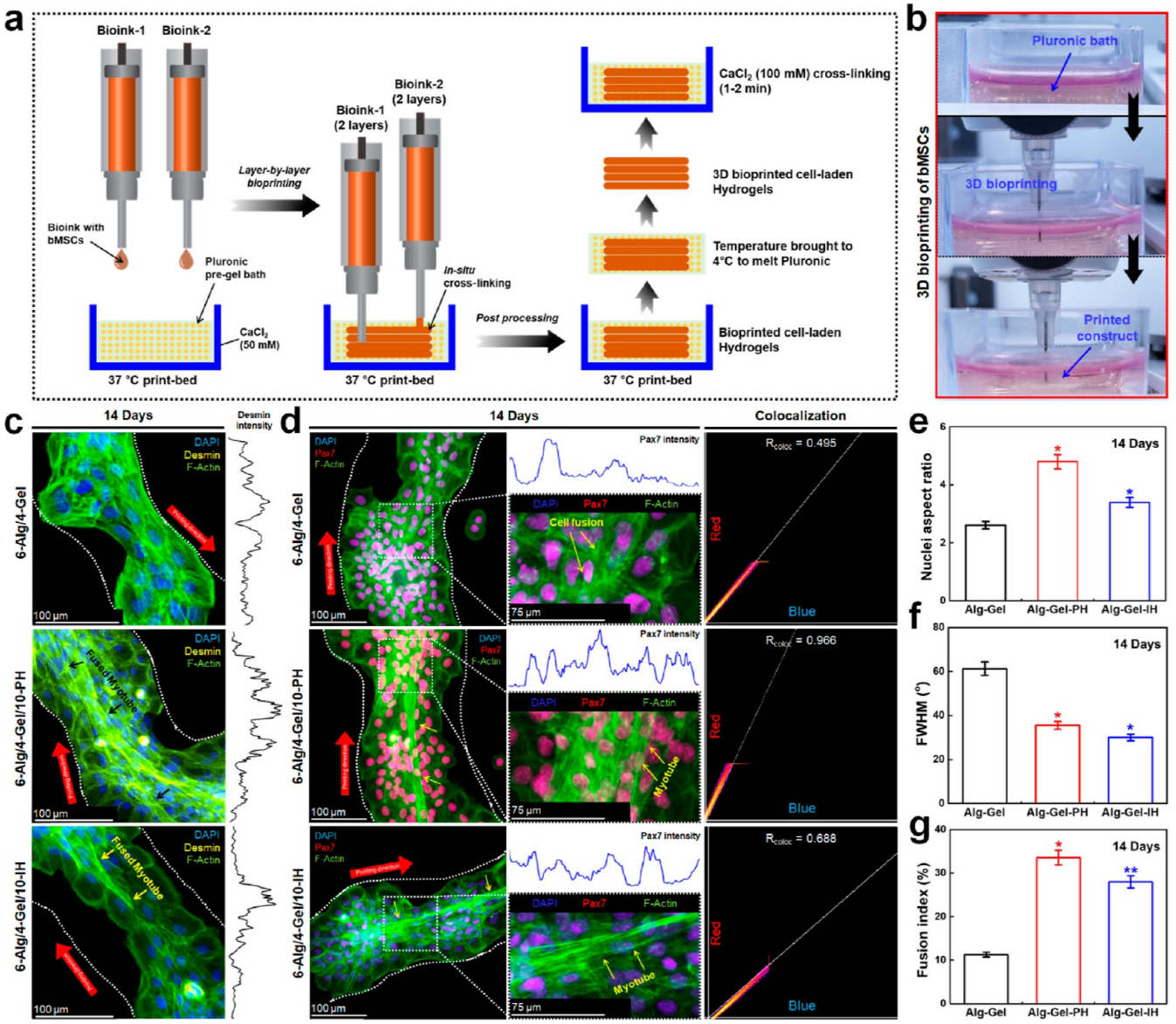

Figure 6. 3D bioprinting of bMSCs using hydrolysate-enriched bioinks for enhanced myogenesis. (a) Schematic illustration of the 3D bioprinting process. (b) Digital photographs showing the 3D printing process within the Pluronic bath. (c) Representative fluorescent microscopy images of the bioprinted bMSCs showing the expression of desmin (yellow) and F-actin (green) after 14 days of myogenic induction. The line-scan profile indicates the relative intensity of desmin. (d) Nuclear localization of Pax7 as an indicator of early myogenesis. The line−scan profile indicates the relative intensity of Pax7. The PCC values for colocalization of Pax7 (red) within the nucleus (DAPI/blue). (e) Aspect ratio (maximum diameter/minimum diameter) of nucleus, FWHM of F-actin arrangement, and fusion index of bMSCs after 14 days of myogenic induction. Scale bar: 75 and 100 μm. Data are mean ± s.d. of triplicate experiments, statistical significance at $^{*}p < 0.05$ and $^{**}p < 0.01$ (Student t-test).

https://doi.org/10.1021/acsami.2c10620
ACS Appl. Mater. Interfaces 2022, 14, 34513−34526

similar observation was noted in the presence of IPHs, where the BPI(NH) supplements exhibited the maximum viability of bMSCs after 48 h of incubation (Figure S12b). None of the IPHs were found to be toxic to the cultured cells, suggesting their biocompatibility. Thus, PHs from plants and insects can be used as a potential alternative to FBS for muscle tissue engineering. Taken together, among the various hydrolysates, SPI(NH) (SPHs) and BPI(NH) (BPHs) exhibited less cytotoxicity and better cell proliferation ability and, therefore, were judiciously chosen for 3D bioprinting of bMSCs.

The myogenic differentiation ability of the SPHs and BPHs was evaluated through ICC analysis, and the results are shown in Figure 5. Interestingly, 10% SPH and BPH supplements exhibited enhanced desmin expression in bMSCs. After 24 h, there was no noticeable change in desmin expression; however, cytoskeletal morphology was profoundly affected following SPH and BPH treatment compared with the control (Figure 5a). Aligned F-actin fibers were observed in both the SPH and BPH treatments, suggesting the potential role of PHs in bMSCs. Interestingly, the bMSCs started to colonize as a larger cell mass after 3 days of culture. bMSCs supplemented with SPHs and BPHs showed radially oriented F-actin fibers with cytoplasmic localization of desmin markers. However, the control group exhibited a poor differentiation ability, with a regular F-actin and desmin morphology. The SPH-treated bMSCs exhibited early cell differentiation, which was characterized by migratory F-actin fibers (Figure S13a). Pax7, an early myogenic marker,[60] was highly expressed after 3 days of culture in a 10% SPH-containing medium. We observed a sudden nuclear accumulation of Pax7 within a fused myotube in the presence of SPHs (Figure S13b), suggesting that the PH supplement significantly induced early myogenesis, as reported previously.[32]

3.6. 3D Printed PH-Enriched Hydrogel Promotes Proliferation of bMSCs. The biocompatibility of the 3D printed hydrogels was evaluated using a live/dead assay after 12 and 24 h of culture. We observed rapid proliferation of cultured cells on the hydrogel surface without any visible cell death (Figure 5b). Strikingly, cellular infiltration on the scaffolds supplemented with PHs (BPHs and IPHs) was significantly higher after 12 h of culture, as evidenced by the higher cell number on the scaffold strand. Our observation is consistent with previous reports where naturally derived protein supplements were used as growth supplements for bovine muscle cells.[7,32]

To investigate the actin morphology of bMSCs, they were grown in DMEM-Glutamax-I medium containing printed 6-Alg/4-Gel, 6-Alg/4-Gel/10-PH, and 6-Alg/4-Gel/10-IH hydrogels for 3 days. The cells were then stained with F-actin and visualized using an inverted fluorescence microscope. As shown in Figure 5c, the bMSCs exhibited normal F-actin morphology without any deformation in the presence of the 6-Alg/4-Gel hydrogel (top image). The line−scan profile indicated an enhanced F-actin intensity. Notably, the bMSCs grown on 6-Alg/4-Gel/10-PH exhibited expanded fiber-like and spindle-shaped actin morphology, confirming that SPH supplementation induced myogenesis in bMSCs. This was confirmed by a decrease in F-actin intensity (middle image). Moreover, the bMSCs grown on the 6-Alg/4-Gel/10-IH hydrogel exhibited a flat F-actin arrangement, indicating the effect of the BPHs (bottom image). The controlled release of PHs from the 6-Alg/4-Gel hydrogel significantly promoted myogenesis of bMSCs. Overall, no structural damage was observed in the cytoskeletal arrangement of the cultured cells, as indicated by immunocytochemistry. This was because of the enhanced bioactivity of the PHs, which favored optimal growth and proliferation of bMSCs.[7,61] Taken together, our results indicate that the developed protein-enriched hydrogels are non-toxic for bMSCs and could be used as a potential alternative for meat analogs in the future. A comparative study on 3D scaffolds with naturally derived extracts for cultured meat production described in the literature is listed in Table 2.

3.7. 3D Bioprinting and Induction of Early Myogenesis. Based on the superior biocompatibility of the developed hydrogel, we aimed to 3D bioprint bMSCs with hydrolysate-enriched bioinks. The 3D bioprinting was performed using 6-Alg/4-Gel, 6-Alg/4-Gel/10-PH, and 6-Alg/4-Gel/10-IH in the presence of a supporting bath system, maintained at a temperature of 37 °C to favor cell viability. We used a 30% Pluronic pre-gel as a supporting bath owing to the fast temperature-dependent gelation and tunable rheological properties (Figure S14). The Pluronic bath was prepared in DMEM supplemented with 50 mM $CaCl_2$, allowing the in situ cross-linking of the Alg-Gel. Prior to 3D printing, each type of bioink containing bMSCs was loaded into two cartridges and incubated at 4 °C to allow gelation. 3D bioprinting was performed layer-by-layer with two printing cartridges in such a way that the first two layers were printed by bioink-1 (hydrogel + bMSCs) and the second two layers were printed by bioink-2 (hydrogel + bMSCs). A schematic overview of the 3D bioprinting process is shown in Figure 6a. The Pluronic pre-gel solution was immediately turned into a gel at 37 °C. Subsequently, a 10 × 10 × 5 mm construct was carefully printed in the Pluronic bath (Figure 6b). We observed excellent printing quality of bMSCs for all bioinks. The extrusion pressures for the 6-Alg/4-Gel, 6-Alg/4-Gel/10-PH, and 6-Alg/4-Gel/10-IH bioinks were 95 ± 2, 72 ± 2, and 75 ± 2 kPa, respectively. As discussed earlier, the PH-enriched bioinks displayed a slight decrease in shear moduli and viscosity; therefore, cell printing with 6-Alg/4-Gel/10-PH and 6-Alg/4-Gel/10-IH required minimal extrusion pressure.

The 3D-bioprinted constructs were carefully transferred to the fresh DMEM/Glutamax-I medium and cultured for 24 h. The viability of the bioprinted bMSCs was evaluated using a live/dead assay, and the results are shown in Figure S15. Interestingly, the bMSCs growing on the 6-Alg/4-Gel/10-PH and 6-Alg/4-Gel/10-IH hydrogels exhibited the highest number of viable cells with a significantly low number of dead cells. In contrast, bioprinted 6-Alg/4-Gel-laden cells exhibited a low number of viable cells. The higher extrusion pressure and low availability of nutrients in the bioprinted 6-Alg/4-Gel likely resulted in low cellular viability.[62,63] Next, we evaluated the myogenic differentiation potential of bioprinted bMSCs after 14 days of incubation using immunocytochemistry to visualize the cytoskeletal morphology (F-actin/green) and desmin (yellow) expression. As shown in Figure 6c, the bioprinted bMSCs in the 6-Alg/4-Gel group exhibited reduced myotube formation and desmin expression. Conversely, the hydrolysate-enriched groups showed several fused myotubes with multiple nuclei. This was also reflected in the line-scan profile, where the relative desmin intensity was significantly higher in hydrolysate-enriched groups than in pure 6-Alg/4-Gel, suggesting that PH supplementation promoted myogenesis. A similar pattern was observed for the Pax7 expression when the bMSCs were cultured under the same conditions for 14 days. The nuclear localization of Pax7 increased significantly

https://doi.org/10.1021/acsami.2c10620
ACS Appl. Mater. Interfaces 2022, 14, 34513−34526

from the pure 6-Alg/4-Gel to the 6-Alg/4-Gel/PHs, suggesting the role of hydrolysates in early myogenesis. To confirm this, we performed a colocalization experiment for Pax7. As shown in Figure 6d, the Pearson's colocalization co-efficient was significantly higher in the 6-Alg/4-Gel/10-PH (R_{coloc} = 0.996) and 6-Alg/4-Gel/10-IH (R_{coloc} = 0.688) hydrogels than that in pure 6-Alg/4-Gel (R_{coloc} = 0.495), conferring the higher expression of Pax7 in the nucleus. Although excellent cell proliferation and myogenesis were observed in all groups, significant cell alignment (nuclear aspect ratio) (Figure 6e) and reduced F-actin arrangement (full-width at half-maximum) (Figure 6f) were observed in the presence of hydrolysate-enriched groups, but not pure 6-Alg/4-Gel. This phenomenon was due to the free availability of the hydrolysates in the bioprinted structure, which promoted bMSC growth and myogenesis, characterized by aggregated or reduced actin orientation and increased fused myotube formation (Figure 6g).

4. CONCLUSIONS

In this study, we developed a technology to surpass the existing limitations of 3D cultured meat using direct ink writing-based 3D bioprinting of an edible polysaccharide (alginate)-protein (gelatin) platform containing naturally derived PHs (plant and insect) for mass proliferation of bMSCs in a low-serum environment. Although cultured meat using livestock-derived muscle and fat cells has drawn significant attention, only a few reports have demonstrated the improved functionality of meat analogues in terms of health and sustainability. In this regard, we demonstrated the successful isolation, culture, and 3D bioprinting of bMSCs using PHs to enhance myogenesis toward fat-free, cleaner, and healthier meat development. The hydrolysates extracted from plants and insects exhibited exceptional antioxidative properties, which favored bMSC proliferation in vitro. The Alg−Gel hydrogel served as a superior platform for 3D printing. The developed 3D bioprinted meat culture platform is simple, easy to fabricate, and eco-friendly, providing an ideal platform for encapsulating proteins and nutrients. Our meat culture platform will provide a new approach for culturing bovine myoblast cells for mass production of CBM in the future.

■ ASSOCIATED CONTENT

Supporting Information

The Supporting Information is available free of charge at https://pubs.acs.org/doi/10.1021/acsami.2c10620.

Characterization of PHs; quantification of SDS-PAGE band intensities for plant and insect PHs; DPPH radical scavenging assay; digital photographs of the DPPH assay; FT-IR spectra of the developed hydrogel scaffolds; rheological properties of the developed bioinks; evaluation of printability of the fabricated bioinks; WST-8 assay of the bMSCs in the presence of PHs; myogenic differentiation of bMSCs in the presence of 10% SPHs; live/dead assay of bMSCs after 24 h of 3D bioprinting; nomenclature of the protein isolates and their corresponding hydrolysates; list of media used for cell culture; nomenclature of hydrogel bioinks used in this study; and primer sequences used for qRT-PCR analysis (PDF)

■ AUTHOR INFORMATION

Corresponding Author

Ki-Taek Lim − *Department of Biosystems Engineering, Kangwon National University, Chuncheon 24341, Republic of Korea; Institute of Forest Science and Interdisciplinary Program in Smart Agriculture, Kangwon National University, Chuncheon 24341, Republic of Korea;* orcid.org/0000-0003-2091-788X; Email: ktlim@kangwon.ac.kr

Authors

Sayan Deb Dutta − *Department of Biosystems Engineering, Kangwon National University, Chuncheon 24341, Republic of Korea*

Keya Ganguly − *Department of Biosystems Engineering, Kangwon National University, Chuncheon 24341, Republic of Korea*

Min-Soo Jeong − *Department of Food Science and Biotechnology, Kangwon National University, Chuncheon 24341, Republic of Korea*

Dinesh K. Patel − *Institute of Forest Science, Kangwon National University, Chuncheon 24341, Republic of Korea*

Tejal V. Patil − *Interdisciplinary Program in Smart Agriculture, Kangwon National University, Chuncheon 24341, Republic of Korea*

Seong-Jun Cho − *Department of Food Science and Biotechnology, Kangwon National University, Chuncheon 24341, Republic of Korea*

Complete contact information is available at: https://pubs.acs.org/10.1021/acsami.2c10620

Author Contributions

S.D.D. and K.G. contributed equally. Conceptualization, methodology, formal analysis, validation, and investigation: S.D.D., K.G., and M.-S.J.; data curation and software: S.D.D., K.G., and T.V.P; writing-original draft; S.D.D. and K.G.; writing-review and editing: D.K.P.; visualization and supervision: S.J.-C. and K.-T.L.; and project administration and funding acquisition: K.-T.L.

Notes

The authors declare no competing financial interest.

■ ACKNOWLEDGMENTS

This work was supported by the Innovative Cultured Meat Technology Development Alchemist Project (20012439), funded by the "Ministry of Trade, Industry, and Energy" (MoTIE, Republic of Korea). This work was also supported by the Basic Science Research Program' through the "National Research Foundation of Korea" funded by the "Ministry of Education" (NRF-2018R1A16A1A03025582, NRF-2019R1D1A3A03103828, and NRF2022R1I1A3063302).

■ REFERENCES

(1) Chen, L.; Guttieres, D.; Koenigsberg, A.; Barone, P. W.; Sinskey, A. J.; Springs, S. L. Large-scale cultured meat production: Trends, challenges and promising biomanufacturing technologies. *Biomaterials* **2022**, *280*, 121274.

(2) Godfray, H. C. J.; Aveyard, P.; Garnett, T.; Hall, J. W.; Key, T. J.; Lorimer, J.; Pierrehumbert, R. T.; Scarborough, P.; Springmann, M.; Jebb, S. A. Meat consumption, health, and the environment. *Science* **2018**, *361*, No. eaam5324.

(3) Stoll-Kleemann, S.; O'Riordan, T. The sustainability challenges of our meat and dairy diets. *Environment* **2015**, *57*, 34−48.

(4) Post, M. J.; Levenberg, S.; Kaplan, D. L.; Genovese, N.; Fu, J.; Bryant, C. J.; Negowetti, N.; Verzijden, K.; Moutsatsou, P. Scientific, sustainability and regulatory challenges of cultured meat. *Nat. Food* **2020**, *1*, 403−415.
(5) Xiang, N.; Yuen, J. S., Jr; Stout, A. J.; Rubio, N. R.; Chen, Y.; Kaplan, D. L. 3D porous scaffolds from wheat glutenin for cultured meat applications. *Biomaterials* **2022**, *285*, 121543.
(6) Macdiarmid, J. I.; Douglas, F.; Campbell, J. Eating like there's no tomorrow: Public awareness of the environmental impact of food and reluctance to eat less meat as part of a sustainable diet. *Appetite* **2016**, *96*, 487−493.
(7) Park, S.; Jung, S.; Heo, J.; Koh, W.-G.; Lee, S.; Hong, J. Chitosan/Cellulose-Based Porous Nanofilm Delivering C-Phycocyanin: A Novel Platform for the Production of Cost-Effective Cultured Meat. *ACS Appl. Mater. Interfaces* **2021**, *13*, 32193−32204.
(8) Slade, P. If you build it, will they eat it? Consumer preferences for plant-based and cultured meat burgers. *Appetite* **2018**, *125*, 428−437.
(9) Ben-Arye, T.; Shandalov, Y.; Ben-Shaul, S.; Landau, S.; Zagury, Y.; Ianovici, I.; Lavon, N.; Levenberg, S. Textured soy protein scaffolds enable the generation of three-dimensional bovine skeletal muscle tissue for cell-based meat. *Nat. Food* **2020**, *1*, 210−220.
(10) Kang, D.-H.; Louis, F.; Liu, H.; Shimoda, H.; Nishiyama, Y.; Nozawa, H.; Kakitani, M.; Takagi, D.; Kasa, D.; Nagamori, E.; Irie, S.; Kitano, S.; Matsusaki, M. Engineered whole cut meat-like tissue by the assembly of cell fibers using tendon-gel integrated bioprinting. *Nat. Commun.* **2021**, *12*, 5059.
(11) Gagaoua, M.; Dib, A. L.; Lakhdara, N.; Lamri, M.; Botineştean, C.; Lorenzo, J. M. Artificial meat tenderization using plant cysteine proteases. *Curr. Opin. Food Sci.* **2021**, *38*, 177−188.
(12) Diarz, E. J.; Leyaro, B. J.; Kivuyo, S. L.; Ngowi, B. J.; Msuya, S. E.; Mfinanga, S. G.; Bonfoh, B.; Mahande, M. J. Red meat consumption and its association with hypertension and hyperlipidaemia among adult Maasai pastoralists of Ngorongoro Conservation Area, Tanzania. *PLoS One* **2020**, *15*, No. e0233777.
(13) Amiano, P.; Chamosa, S.; Etxezarreta, N.; Arriola, L.; Sánchez, M.; Ardanaz, E.; Molina-Montes, E.; Chirlaque, M.; Moreno-Iribas, C.; Huerta, J.; Egües, N.; Navarro, C.; Requena, M.; Quirós, J.-R.; Fonseca-Nunes, A.; Jakszyn, P.; González, C.-A.; Dorronsoro, M. Unprocessed red meat and processed meat consumption and risk of stroke in the Spanish cohort of the European Prospective Investigation into Cancer and Nutrition (EPIC). *Eur. J. Clin. Nutr.* **2016**, *70*, 313−319.
(14) Dolan, L.; Smith, K. S.; Marlin, M. B.; Bell, L. N.; Blythe, E.; Greene, M. W.; Frugé, A. D. Food security, obesity, and meat-derived carcinogen exposure in US adults. *Food Chem. Toxicol.* **2021**, *155*, 112412.
(15) Abu-Halaka, D.; Gover, O.; Rauchbach, E.; Zelber-Sagi, S.; Schwartz, B.; Tirosh, O. Whole body metabolism is improved by hemin added to high fat diet while counteracted by nitrite: a mouse model of processed meat consumption. *Food Funct.* **2021**, *12*, 8326.
(16) Heffernan, O. Sustainability: A meaty issue. *Nature* **2017**, *544*, S18−S20.
(17) Bodiou, V.; Moutsatsou, P.; Post, M. J. Microcarriers for upscaling cultured meat production. *Front. Nutr.* **2020**, *7*, 10.
(18) Post, M. J. Cultured meat from stem cells: Challenges and prospects. *Meat Sci.* **2012**, *92*, 297−301.
(19) Arshad, M. S.; Javed, M.; Sohaib, M.; Saeed, F.; Imran, A.; Amjad, Z. Tissue engineering approaches to develop cultured meat from cells: a mini review. *Cogent Food Agric.* **2017**, *3*, 1320814.
(20) Dryáková, A.; Pihlanto, A.; Marnila, P.; Čurda, L.; Korhonen, H. J. Antioxidant properties of whey protein hydrolysates as measured by three methods. *Eur. Food Res. Technol.* **2010**, *230*, 865−874.
(21) Liao, X.; Zhu, Z.; Wu, S.; Chen, M.; Huang, R.; Wang, J.; Wu, Q.; Ding, Y. Preparation of Antioxidant Protein Hydrolysates from Pleurotus geesteranus and Their Protective Effects on H2O2 Oxidative Damaged PC12 Cells. *Molecules* **2020**, *25*, 5408.
(22) Halliwell, B.; Murcia, M. A.; Chirico, S.; Aruoma, O. I. Free radicals and antioxidants in food and in vivo: what they do and how they work. *Crit. Rev. Food Sci. Nutr.* **1995**, *35*, 7−20.
(23) Zhang, Q.; Wu, C.; Fan, G.; Li, T.; Sun, Y. Improvement of antioxidant activity of Morchella esculenta protein hydrolysate by optimized glycosylation reaction. *CyTA—J. Food* **2018**, *16*, 238−246.
(24) Tkaczewska, J.; Borawska-Dziadkiewicz, J.; Kulawik, P.; Duda, I.; Morawska, M.; Mickowska, B. The effects of hydrolysis condition on the antioxidant activity of protein hydrolysate from Cyprinus carpio skin gelatin. *LWT* **2020**, *117*, 108616.
(25) Tsuruwaka, Y.; Shimada, E. Reprocessing seafood waste: challenge to develop aquatic clean meat from fish cells. *NPJ Sci. Food* **2022**, *6*, 7.
(26) Saiga, A.; Tanabe, S.; Nishimura, T. Antioxidant activity of peptides obtained from porcine myofibrillar proteins by protease treatment. *J. Agric. Food Chem.* **2003**, *51*, 3661−3667.
(27) Park, E. Y.; Murakami, H.; Mori, T.; Matsumura, Y. Effects of protein and peptide addition on lipid oxidation in powder model system. *J. Agric. Food Chem.* **2005**, *53*, 137−144.
(28) Pihlanto, A.; Akkanen, S.; Korhonen, H. J. ACE-inhibitory and antioxidant properties of potato (Solanum tuberosum). *Food Chem.* **2008**, *109*, 104−112.
(29) Olagunju, A. I.; Omoba, O. S.; Enujiugha, V. N.; Alashi, A. M.; Aluko, R. E. Pigeon pea enzymatic protein hydrolysates and ultrafiltration peptide fractions as potential sources of antioxidant peptides: An in vitro study. *LWT* **2018**, *97*, 269−278.
(30) Ganguly, K.; Jeong, M.-S.; Dutta, S. D.; Patel, D. K.; Cho, S.-J.; Lim, K.-T. Protaetia brevitarsis seulensis Derived Protein Isolate with Enhanced Osteomodulatory and Antioxidative Property. *Molecules* **2020**, *25*, 6056.
(31) García, M.; Puchalska, P.; Esteve, C.; Marina, M. Vegetable foods: A cheap source of proteins and peptides with antihypertensive, antioxidant, and other less occurrence bioactivities. *Talanta* **2013**, *106*, 328−349.
(32) Ianovici, I.; Zagury, Y.; Redenski, I.; Lavon, N.; Levenberg, S. 3D-printable plant protein-enriched scaffolds for cultivated meat development. *Biomaterials* **2022**, *284*, 121487.
(33) Chien, K. B.; Shah, R. N. Novel soy protein scaffolds for tissue regeneration: Material characterization and interaction with human mesenchymal stem cells. *Acta Biomater.* **2012**, *8*, 694−703.
(34) Chen, J.; Sun, H.; Mu, T.; Blecker, C.; Richel, A.; Richard, G.; Jacquet, N.; Haubruge, E.; Goffin, D. Effect of temperature on rheological, structural, and textural properties of soy protein isolate pastes for 3D food printing. *J. Food Eng.* **2022**, *323*, 110917.
(35) Dutta, S. D.; Hexiu, J.; Patel, D. K.; Ganguly, K.; Lim, K.-T. 3D-printed bioactive and biodegradable hydrogel scaffolds of alginate/gelatin/cellulose nanocrystals for tissue engineering. *Int. J. Biol. Macromol.* **2021**, *167*, 644−658.
(36) Hong, S.; Kim, J. S.; Jung, B.; Won, C.; Hwang, C. Coaxial bioprinting of cell-laden vascular constructs using a gelatin−tyramine bioink. *Biomater. Sci.* **2019**, *7*, 4578−4587.
(37) Yoon, S.; Wong, N. A.; Chae, M.; Auh, J.-H. Comparative characterization of protein hydrolysates from three edible insects: Mealworm larvae, adult crickets, and silkworm pupae. *Foods* **2019**, *8*, 563.
(38) Dutta, S. D.; Bin, J.; Ganguly, K.; Patel, D. K.; Lim, K.-T. Electromagnetic field-assisted cell-laden 3D printed poloxamer-407 hydrogel for enhanced osteogenesis. *RSC Adv.* **2021**, *11*, 20342−20354.
(39) Ketnawa, S.; Benjakul, S.; Martínez-Alvarez, O.; Rawdkuen, S. Fish skin gelatin hydrolysates produced by visceral peptidase and bovine trypsin: Bioactivity and stability. *Food Chem.* **2017**, *215*, 383−390.
(40) Kamnerdpetch, C.; Weiss, M.; Kasper, C.; Scheper, T. An improvement of potato pulp protein hydrolyzation process by the combination of protease enzyme systems. *Enzyme Microb. Technol.* **2007**, *40*, 508−514.

(41) Udenigwe, C. C.; Aluko, R. E. Chemometric analysis of the amino acid requirements of antioxidant food protein hydrolysates. *Int. J. Mol. Sci.* **2011**, *12*, 3148−3161.
(42) Udenigwe, C. C. Bioinformatics approaches, prospects and challenges of food bioactive peptide research. *Trends Food Sci. Technol.* **2014**, *36*, 137−143.
(43) Yang, R.; Li, X.; Lin, S.; Zhang, Z.; Chen, F. Identification of novel peptides from 3 to 10 kDa pine nut (Pinus koraiensis) meal protein, with an exploration of the relationship between their antioxidant activities and secondary structure. *Food Chem.* **2017**, *219*, 311−320.
(44) Liu, Y.; Hu, Q.; Dong, W.; Liu, S.; Zhang, H.; Gu, Y. Alginate/Gelatin-based Hydrogel with Soy Protein/peptide Powder for 3D Printing Tissue-engineering Scaffolds to Promote Angiogenesis. *Macromol. Biosci.* **2022**, *22*, 2100413.
(45) Rastogi, P.; Kandasubramanian, B. Review of alginate-based hydrogel bioprinting for application in tissue engineering. *Biofabrication* **2019**, *11*, 042001.
(46) Schwab, A.; Levato, R.; D'Este, M.; Piluso, S.; Eglin, D.; Malda, J. Printability and shape fidelity of bioinks in 3D bioprinting. *Chem. Rev.* **2020**, *120*, 11028−11055.
(47) Marchesan, S.; Qu, Y.; Waddington, L. J.; Easton, C. D.; Glattauer, V.; Lithgow, T. J.; McLean, K. M.; Forsythe, J. S.; Hartley, P. G. Self-assembly of ciprofloxacin and a tripeptide into an antimicrobial nanostructured hydrogel. *Biomaterials* **2013**, *34*, 3678−3687.
(48) Highley, C. B.; Rodell, C. B.; Burdick, J. A. Direct 3D printing of shear-thinning hydrogels into self-healing hydrogels. *Adv. Mater.* **2015**, *27*, 5075−5079.
(49) Loebel, C.; Rodell, C. B.; Chen, M. H.; Burdick, J. A. Shear-thinning and self-healing hydrogels as injectable therapeutics and for 3D-printing. *Nat. Protoc.* **2017**, *12*, 1521−1541.
(50) Gao, T.; Gillispie, G. J.; Copus, J. S.; Pr, A. K.; Seol, Y.-J.; Atala, A.; Yoo, J. J.; Lee, S. J. Optimization of gelatin−alginate composite bioink printability using rheological parameters: a systematic approach. *Biofabrication* **2018**, *10*, 034106.
(51) Shahbazi, M.; Jäger, H.; Ettelaie, R.; Chen, J. Construction of 3D printed reduced-fat meat analogue by emulsion gels. Part I: Flow behavior, thixotropic feature, and network structure of soy protein-based inks. *Food Hydrocolloids* **2021**, *120*, 106967.
(52) Lin, S.; Liu, J.; Liu, X.; Zhao, X. Muscle-like fatigue-resistant hydrogels by mechanical training. *Proc. Natl. Acad. Sci. U.S.A.* **2019**, *116*, 10244−10249.
(53) Gholobova, D.; Terrie, L.; Gerard, M.; Declercq, H.; Thorrez, L. Vascularization of tissue-engineered skeletal muscle constructs. *Biomaterials* **2020**, *235*, 119708.
(54) Bomkamp, C.; Skaalure, S. C.; Fernando, G. F.; Ben-Arye, T.; Swartz, E. W.; Specht, E. A. Scaffolding Biomaterials for 3D Cultivated Meat: Prospects and Challenges. *Adv. Sci.* **2022**, *9*, 2102908.
(55) Patel, D. K.; Dutta, S. D.; Hexiu, J.; Ganguly, K.; Lim, K.-T. 3D-printable chitosan/silk fibroin/cellulose nanoparticle scaffolds for bone regeneration via M2 macrophage polarization. *Carbohydr. Polym.* **2022**, *281*, 119077.
(56) Cheng, Y.; Shi, X.; Jiang, X.; Wang, X.; Qin, H. Printability of a cellulose derivative for extrusion-based 3D printing: The application on a biodegradable support material. *Front. Mater.* **2020**, *7*, 86.
(57) Smith, C.; Janney, M.; Allen, R. Temporal expression of myogenic regulatory genes during activation, proliferation, and differentiation of rat skeletal muscle satellite cells. *J. Cell. Physiol.* **1994**, *159*, 379−385.
(58) Iwanaga, K.; Murata, T.; Okada, M.; Hori, M.; Ozaki, H. Carbachol induces Ca2+-dependent contraction via muscarinic M2 and M3 receptors in rat intestinal subepithelial myofibroblasts. *J. Pharmacol. Sci.* **2009**, *110*, 306−314.
(59) Iwanaga, K.; Murata, T.; Hori, M.; Ozaki, H. Isolation and characterization of bovine intestinal subepithelial myofibroblasts. *J. Pharmacol. Sci.* **2010**, *112*, 98−104.
(60) Wen, Y.; Bi, P.; Liu, W.; Asakura, A.; Keller, C.; Kuang, S. Constitutive Notch activation upregulates Pax7 and promotes the self-renewal of skeletal muscle satellite cells. *Mol. Cell. Biol.* **2012**, *32*, 2300−2311.
(61) Messmer, T.; Klevernic, I.; Furquim, C.; Ovchinnikova, E.; Dogan, A.; Cruz, H.; Post, M. J.; Flack, J. E. A serum-free media formulation for cultured meat production supports bovine satellite cell differentiation in the absence of serum starvation. *Nat. Food* **2022**, *3*, 74.
(62) Chang, R.; Nam, J.; Sun, W. Effects of dispensing pressure and nozzle diameter on cell survival from solid freeform fabrication−based direct cell writing. *Tissue Eng., Part A* **2008**, *14*, 41−48.
(63) Blaeser, A.; Duarte Campos, D. F.; Puster, U.; Richtering, W.; Stevens, M. M.; Fischer, H. Controlling shear stress in 3D bioprinting is a key factor to balance printing resolution and stem cell integrity. *Adv. Healthcare Mater.* **2016**, *5*, 326−333.

https://doi.org/10.1021/acsami.2c10620
ACS Appl. Mater. Interfaces 2022, 14, 34513−34526